

**CFA '18 LE HAVRE ■ 23-27 avril 2018**  
**14<sup>ème</sup> Congrès Français d'Acoustique**



**Comportement d'un liner acoustique par approche de type Lattice Boltzmann**

F. Simon<sup>a</sup>, P. Marchner<sup>b</sup>, R. Roncen<sup>b</sup> et F. Chevillotte<sup>c</sup>

<sup>a</sup>ONERA-The French Aerospace Lab, 2 Avenue Edouard Belin, 31055 Toulouse, France

<sup>b</sup>ONERA, 2 avenue Edouard Belin, 31055 Toulouse, France

<sup>c</sup>MATELYS, 7 rue des maraîchers, Bât B, 69120 Vaulx-En-Velin, France  
frank.simon@onera.fr

The absorbent materials (called liner) used in engine nacelles to reduce fan noise, are Helmholtz resonator type and have perforated walls glued to a honeycomb placed on a reflective background. The ratio "wall thickness / hole diameter" generally around 1 makes the acoustic impedance dependent on the incident sound level and grazing flow, to the detriment of the optimal design. The linear behavior, mainly based on the viscous friction within the holes, is relatively well described by the (semi)-empirical models, while the nonlinear effects due to the generation and shedding of acoustic vortices at the periphery of the holes require a numerical approach to introduce correction terms into the models (eg via a discharge coefficient). In this sense, the resolution of the Boltzmann equation at the mesoscopic scale constitutes an alternative to the direct numerical simulation (DNS) of the compressible Navier-Stokes equations. This paper describes the numerical model associated with the study of a liner, the calculation process and the information derived from the ProLB software implemented by Matelys. An analysis of the non-linear effects due to the incident pressure level is conducted for two liners configurations. It appears, on the one hand, that this type of approach is particularly well suited to intensive computing (eg computing with 10 to 15 million cells in a few hours) and, on the other hand, that visualization of the flow within an orifice, the development of the acoustic boundary layer and the recirculation zones are well captured. It could thus be used in the future to achieve the "design" of materials with a goal of linearity in a given level range.

## 1 Introduction

Locally reacting liners, as those used in aeronautical engine nacelles, are generally "sandwich" resonators with a perforated plate linked to an honeycomb material above a rigid plate. Their acoustic absorption can be simply explained by the principle of an Helmholtz resonator. The frequency range of absorption is essentially controlled by the thickness of honeycomb cavity (reactance effect), while the small size of holes brings a resistance to acoustic waves. This behavior, mainly based on the viscous friction within the holes, is relatively well described by the (semi) - empirical models. Nevertheless, the acoustic impedance can depend non linearly on the incident particle velocity level. Thus, above a threshold value of the ratio "particle velocity / friction velocity", a vortex shedding can be produced periodically from both ends of each hole [1,2].

According to Melling [3], nonlinearities develop when the Reynolds number in the orifice is in the order of  $30 < Re < 2000$ . In [4], Temiz concludes that non linearities effects become significant when the Strouhal number in the orifice is in the order of unity.

To describe this phenomenon, Melling [3] proposed to add a nonlinear resistance correction to the linear model as following:

$$R = \frac{1}{\rho c} \left( R_{lin} + \frac{8}{3\pi} \left[ \frac{1}{C_D^2} \left( \frac{1-\phi^2}{\phi^2} \right) V_n \frac{\rho}{2} \right] \right) \quad (1)$$

with  $R_{lin}$  the real part of linear acoustic impedance,  $V_n$  the amplitude of acoustic velocity and  $C_D$  called discharge coefficient.

$C_D$ , difficult to quantify, is a nondimensional number used to describe the flow contraction in the perforation. It might depend on the excitation frequency, the Reynolds number or the geometry of the orifice [5].

The non-linear correction of reactance, often interpreted as losses of the attached mass due to sound pressure level increase, should depend on Reynolds number and porosity [3].

In practical terms, CFD simulations can be an alternative to experiments to determine the suitable correction terms into the models (eg via a discharge coefficient). Nevertheless, it remains a challenge because of the refined mesh that must be designed in order to capture the flow effects.

In this sense, the resolution of the Boltzmann equation at the mesoscopic scale applied to perforated plates constitutes a new interesting approach. This paper describes

the numerical model associated with the study of a liner and the calculation process with ProLB software. An analysis of the non-linear effects due to the incident pressure level is conducted for two liners configurations. Finally, an experimental validation of velocity field is led in an aeroacoustic test bench equipped with LDV system.

## 2 Boltzmann approach for flow description

Boltzmann equation deals with statistical mechanics. It uses a so-called mesoscopic description of the matter. This physical point of view is between a macroscopic description, such as continuous fluid mechanics and a microscopic particle approach. At this scale, the relevant physical quantity is the particle probability density function  $f(x, c, t)$ . It is a statistical distribution of a high number of particles with  $c$  the particle velocity and  $x$  the vector for space coordinates.

For instance,  $f(x, c, t) dx dc$  is the probability to find a particle at time  $t$  with a speed between  $c$  and  $c + dc$  in the neighborhood of  $x$ . For convenience,  $f(x, c, t)$  will be noted by  $f$ . The original Boltzmann equation describes the transport of this particle distribution function. The 3D Boltzmann equation can be written as:

$$\frac{\partial f}{\partial t} + c_i \frac{\partial f}{\partial x_i} + \frac{F_i}{m} \frac{\partial f}{\partial c_i} = C(f) \quad (2)$$

The subscript  $i$  represent the 3 space directions  $x, y$  and  $z$ .  $F$  is an external force such as gravity,  $m$  the mass of a single particle and  $C(f)$  the collision operator. By neglecting external forces contribution, the Boltzmann equation can be rewritten:

$$\frac{\partial f}{\partial t} + c_i \frac{\partial f}{\partial x_i} = -\frac{1}{\tau} (f - f_{eq}) \quad (3)$$

with  $f_{eq}$  the Maxwell-Boltzmann distribution at equilibrium and  $\tau$  linked to the kinematic viscosity of the fluid. The fluid macroscopic variables such as density  $\rho(x, t)$ , fluid velocity  $u(x, t)$  and the internal energy of the gas  $e(x, t)$  can be retrieved by computing the moment of order 0, 1 and 2 of the probability distribution function.

It is common to assume that the particles can only move in a finite number of directions. This leads to restrict the velocity space into a discrete number of velocities. Then,

the space is divided into a finite number of bounded cells. Each cell contains a central node with the distribution function information. Lattice Boltzmann Methods are associated with numerical schemes called  $DnQm$ , where  $n$  is the space dimension and  $m$  the number of discrete velocities. These considerations lead to the so-called Discrete Velocity Boltzmann Equation (DVBE):

$$\frac{\partial f_\alpha}{\partial t} + c_{\alpha,i} \frac{\partial f_\alpha}{\partial x_i} = -\frac{1}{\tau} (f_\alpha - f_{\alpha,eq}) \quad (4)$$

$\alpha$  is the index representing the number of discrete velocities.

In the discrete velocity model,  $f_\alpha$  is expressed as a projection of  $f$  on Hermite polynomials. Thanks to this development, the coefficients of the polynomial basis appear to be the momentums of the distribution function  $f$ . The discrete equilibrium distribution  $f_{\alpha,eq}$  needs to be approximated by a Taylor expansion for low velocities and can then be expressed as a development in Hermite polynomials:

$$f_{\alpha,eq} = \rho \omega_\alpha \left( 1 + \frac{u \cdot c_\alpha}{rT} + \frac{(u \cdot c_\alpha)^2}{(rT)^2} - \frac{|u|^2}{2(rT)} + \vartheta(u^3) \right) \quad (5)$$

with  $r$  the specific gas constant and  $\omega_\alpha$  weighting coefficients from the Hermite polynomial truncation. The fluid velocity approximate at  $\vartheta(u^3)$  makes LBM simulations only valid at low Mach numbers.

To sum up, a Lattice Boltzmann scheme is characterized by weighting coefficients and a set of discrete velocities  $c_\alpha$ . In the restricted velocity space, the macroscopic variables take the following form:

$$\begin{cases} \rho = \sum_\alpha f_\alpha \\ \rho u = \sum_\alpha c_\alpha f_\alpha \\ \rho e + \frac{1}{2} \rho |u|^2 = \sum_\alpha |c_\alpha|^2 f_\alpha \end{cases} \quad (6)$$

The time discretization can be regarded as an explicit scheme of second order in time.

In this study, the ProLB solver uses a direct method for computational aeroacoustics based on the Lattice Boltzmann Method described above. ProLB-Porous is a module specifically implemented by Matelys for studying porous media.

### 3 Application to liners

#### 3.1 Simulation results and analysis for a generic liner

Let us consider a generic acoustic liner whose parameters and associated numerical model are respectively presented in Table 1 and Figure 1.

Table 1: Liner parameters used for numerical simulations

Hole radius r (mm)	Cavity length $L_{cav}$ (mm)	Plate Porosity $\phi$	Plate thickness d (mm)
0.15	20	5%	0.8

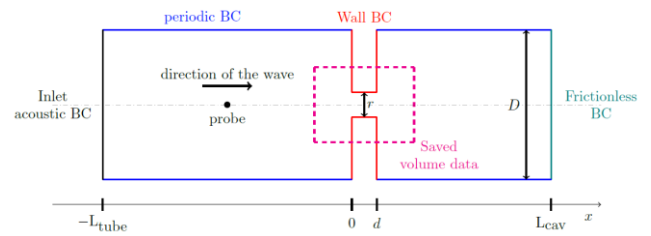


Figure 1: LBM model with ProLB for the simulation of a single perforation above a cavity subjected to harmonic or broadband excitation. Drawing is not to scale.

As shown in Figure 1, the different boundary conditions (BC) are:

- Inlet acoustic boundary condition: an acoustic velocity is set up as input. It can either be a pure sine tone for harmonic analysis or a linear chirp for broadband frequency computations.
- Periodic boundary condition
- Wall boundary condition: It is a no-slip condition. The velocity at the wall is zero.
- Frictionless boundary condition: It is a free-slip condition. The normal velocity component at the wall is zero.
- Sponge zones: These are buffer zones defined to avoid spurious reflections at the boundaries. A damping function is used and its value changes dynamically with the knowledge of the local velocity [7].

The mesh generation is set up in a cartesian manner. Cells are built within a central node in both the fluid simulation and boundary condition volumes.

A criterion to estimate the mesh accuracy is the adimensional wall distance  $y^+$ . It gives an apriori estimate of the flow effects that could be captured by the simulation. In the present work,  $y^+$  of the nearest cell at the orifice wall is evaluated. Usually, DNS computations recommend the range  $0 < y^+ < 3$ .

The adimensional wall distance  $y^+$  is defined as in [7]:

$$y^+ = \rho \frac{y_{mesh}}{\mu} u_{jet} \sqrt{\frac{C_f}{2}} \quad (7)$$

with  $C_f = (2 \log(Re) - 0.65)^{-2.3}$ , the Schlichting skin friction,  $y_{mesh}$ , the mesh size and  $u_{jet}$ , the jet velocity defined by  $\frac{1}{\phi C_D} V_n$ .

Three mesh refinement regions are used. Due to the solver architecture, the ratio between the meshing regions must be related by of a factor of two. A typical mesh used for the computations is illustrated in Figure 2.

Popie [9] recommends defining around 15 points in the viscous boundary layer whose the thickness  $\delta$  can be evaluated by  $\delta = \sqrt{\frac{2\mu}{\rho\omega}}$

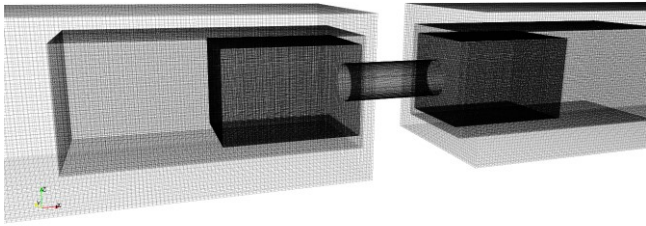


Figure 2: Sample of the mesh. The mesh is built with 3 refinement regions. The orifice diameter is meshed by 50 cells. The mesh size are respectively  $6\ \mu\text{m}$ ,  $12\ \mu\text{m}$  and  $24\ \mu\text{m}$ .

The orifice diameter is meshed by 50 cells. Depending on the excitation frequency, the viscous boundary layer will contain from 10 to 16 cells. The cell size in the orifice is  $6\ \mu\text{m}$  and the model contains 15 million nodes.

Three frequencies are computed: 1600, 2500 and 4000 Hz. 2500 Hz is close to the liner resonance frequency with the linear model.

The computations are launched for SPLs starting from 110 dB until 170 dB with a step of 10dB. For each calculation, time data are saved during a couple of periods of the input sinus. The Figures 3 and 4 illustrate the values taken by commonly used adimensional numbers for the investigated configurations under harmonic excitation. The Strouhal Reynolds, Helmholtz and Shear numbers are plotted.  $y^+$  values are computed for the first wall cell.

Between 120 and 130dB, the Strouhal number is in the order of unity. Nonlinear behaviour should be initiated [5]. At 170dB, the high  $y^+$  value might lead to erroneous simulations.

As described in introduction, the linear response corresponds to an "oscillating mass" behavior. Nonlinear response can be identified by the production of vortices at the aperture: A vortex is created when the pressure increases at one orifice end. After the vortex production, the pressure grows on the opposite side. The flow is suctioned until the opposite orifice end and a new vortex is produced. The acoustic cycle is completed.

The time domain evolution of the flow field behavior is presented for three configurations: 110dB-2500Hz, 130 dB-2500 Hz and 160 dB-4000 Hz.

The Figures 5 to 8 show two scalar fields:

- on top, the velocity magnitude field. Arrows represent the direction of the velocity vector.
- on bottom, the vorticity magnitude field. Contours represents the Q-criterion. The Q-criterion is a vortex identification technique. With this criterion, vortices are defined as areas where the vorticity magnitude is greater than the strain rate magnitude [10].

For each picture, the associated x-velocity profile is plotted at the center of the orifice.

At 110dB (Figure 5), an acoustic cycle of the "oscillating mass" effect can be visualized. First, the orifice radiates sound into the cavity. Secondly, flow reversal occurs in the viscous boundary layer. Recirculation zones appear due to the velocity difference between the center of the orifice and the viscous boundary layer. To finish, the flow recirculation zone is completely suctioned and the orifice radiates sound on the other side.

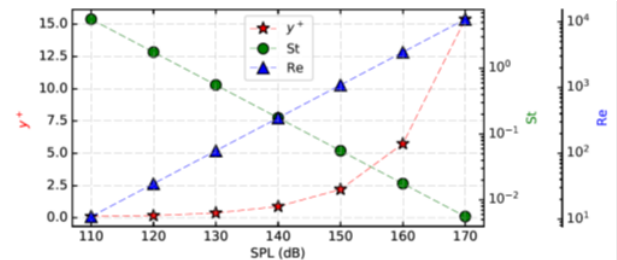


Figure 3: Reynolds,  $y^+$  and Strouhal numbers as function of the simulated excitation levels. The Strouhal number is taken at 2500 Hz.

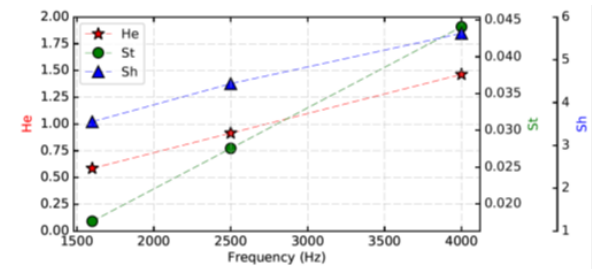


Figure 4: Helmholtz, Shear and Strouhal number as function of simulated frequencies. The Strouhal number is taken at 160dB.

Let us examine the flow field evolution for the configuration at 130dB-2500Hz over an acoustic cycle (Figure 6). On the first picture, the flow within the orifice reaches its maximal speed. Flow recirculation is observed at the aperture. Unlike the situation at 110dB, the velocity is high enough to eject these flow recirculations out of the perforation. Viscous strength is too weak to hold the flow inertia. At the aperture, the flow interacts with the surrounding low speed medium and creates a vortex.

The size of the vortex increases over time: first, the vortex stays compact and grows by the conversion of kinetic energy into vorticity. Then, the vorticity energy is spread out by the air viscosity. The arrows help to visualize the two different phases.

For the configuration at 160dB-4000Hz (Figure 7), the vortex generation is shorter in time but the vorticity magnitude is higher. The generation and the dissipation of the vortex is similar to the case at 130 dB-2500 Hz. The shape of the viscous boundary layer is changed because the velocity magnitude within the orifice is higher. At 110dB, the flow recirculation has no effect on the acoustic radiation. At 130dB, pictures show that a large part of the kinetic energy of the flow is stored in the vortex. The vortex has received acoustical energy and will dissipate it by visco-thermal effects in the far field region. At 160dB, the kinetic energy of the flow and the converted vorticity energy are higher compared to the case at 130dB. However, the vorticity energy generated compared to the initial kinetic energy is lower, leading to a less efficient acoustic absorption.

The Figure 8 shows the SPL influence on the flow field in the orifice neighborhood. Each picture is plotted at the same time and frequency.

At 120dB, extra mass flow is ejected from the aperture. However, a part of the ejected mass is suctioned due to flow reversal. It marks the transition with nonlinearity. This state will be called "weak" nonlinearity.

From 130dB to 160dB, the vortices are growing with SPL.

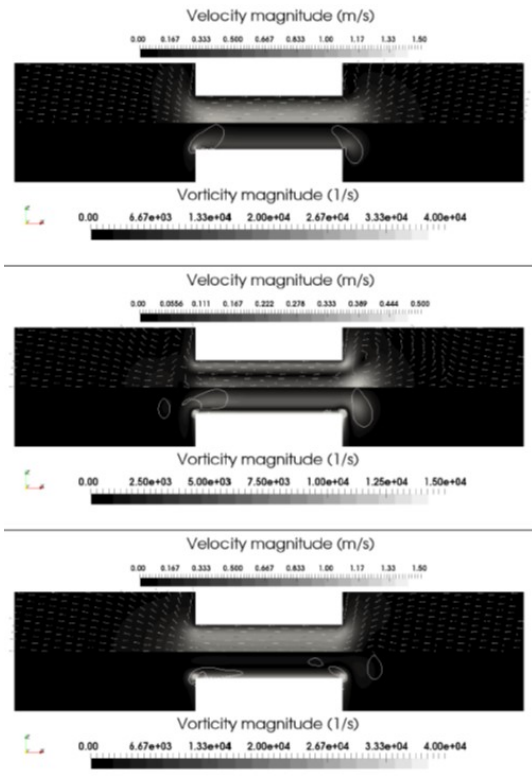


Figure 5: Time evolution at 110 dB and 2500 Hz. Velocity and vorticity magnitude fields. Flow direction and Q-criterion. The time interval between each picture is  $\Delta t = 50\mu s$ .

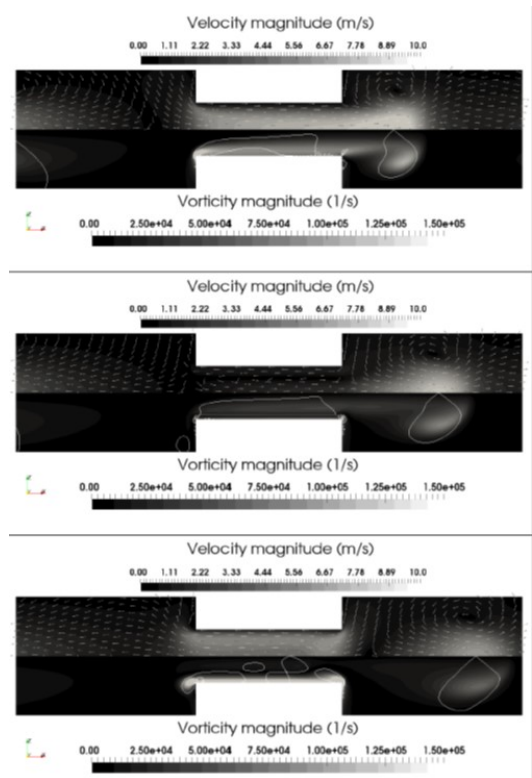


Figure 6: Time evolution at 130 dB and 2500 Hz. Velocity and vorticity magnitude fields. Flow direction and Q-criterion. The time interval between each picture is  $\Delta t = 50\mu s$ .

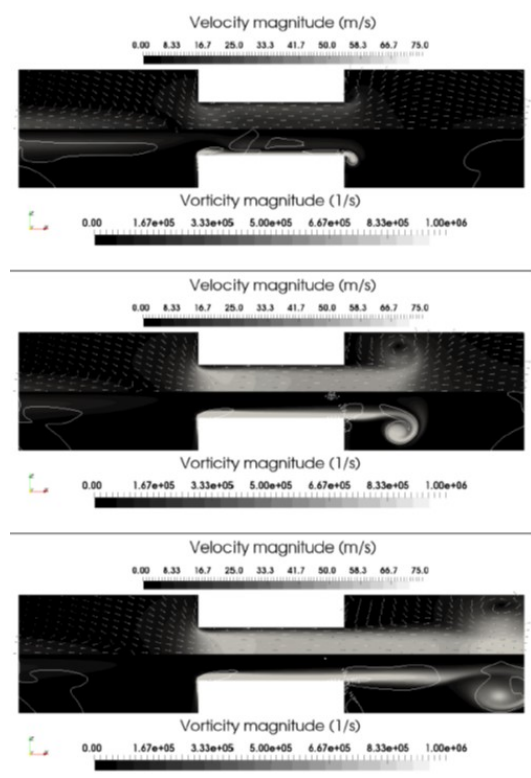


Figure 7: Time evolution at 160 dB and 4000 Hz. Velocity and vorticity magnitude fields. Flow direction and Q-criterion. The time interval between each picture is  $\Delta t = 50\mu s$ .

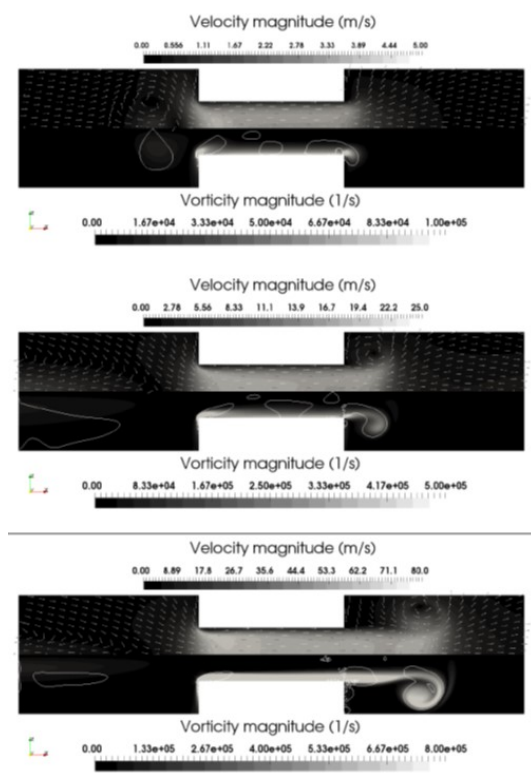


Figure 8: SPL evolution of velocity and vorticity fields at 2500 Hz at a fixed time. Arrows represent the flow direction and contours of Q-criterion are plotted. From up to bottom: 120, 140 and 160 dB.

Finally, the figure 9 presents the global absorption coefficient, normalized resistance and reactance. The results have been obtained by the two microphone transfer function method. As noticed previously, the beginning of

the nonlinear behavior depends on the frequency. The highest absorption value is reached when the part of kinetic energy converted into vorticity is optimal. This can be observed in Figures 6 and 7. For instance, at 140dB and 2500 Hz, the situation is specific: no flow is suctioned by the flow reversal and no extra flow is ejected by an oversupply of kinetic energy. The optimal energy conversion is achieved. The resonance helps the absorption to remain high. However, the vorticity acoustic absorption process is more efficient at 4000 Hz than at 2500 Hz. The resistivity increases with the SPL. At 150 dB, the highest value of resistivity is attained by the case at 1600 Hz. The resistivity rises because the total flow rate within the orifice in an acoustic period is higher. The reactance slowly decreases from 120 to 140 dB. Despite the SPL increases, the mass involved in the acoustic radiation remains constant or slowly decrease. When the acoustic excitation level is too high, the reactance takes higher values and badly impacts the absorption coefficient.

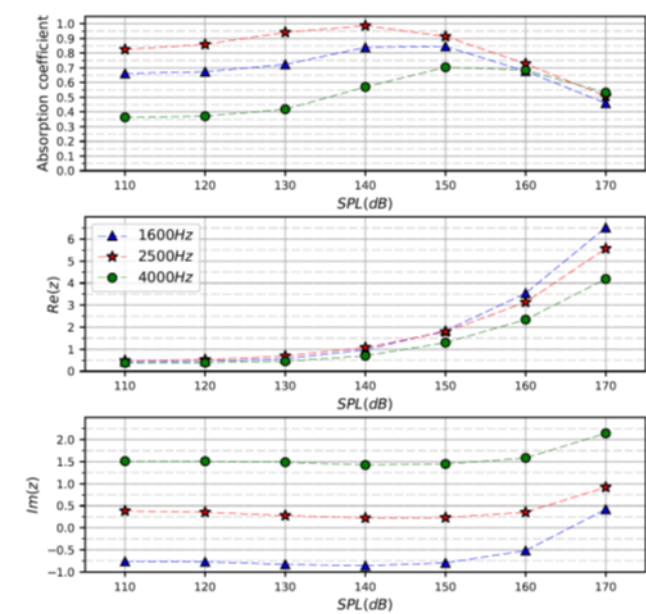


Figure 9: Absorption coefficient, acoustic normalized resistance and reactance as a function of SPL for 1600, 2500 and 4000 Hz.

### 3.2 Simulation results and analysis for a real liner

In this section, a LBM model is carried out in a configuration of liner (Table 2) designed by Airbus and tested in an Onera Test bench called B2A in the frame of EFAPS2 project. Experimental results have already been provided in [10].

Table 2: Liner parameters used for numerical simulations

Hole radius r (mm)	Cavity length $L_{cav}$ (mm)	Plate Porosity $\phi$	Plate thickness d (mm)
0.55	30	9%	0.8

The duct (Figure 10) has a cross-sectional geometry of 50 mm x 50 mm. The 200 mm-long test section is equipped with two silica windows for optical access, allowing two-

components Laser Doppler Velocimetry (LDV) measurements. The emitting optics produce a 50  $\mu$ m-diameter measurement volume. Flow is seeded with incense smoke. Two acoustic drivers are mounted upstream of the test section, and are used to generate tones (multi-sine signal) at up to 140 dB over a frequency range of 300 to 3400 Hz. The signal processing applied to extract acoustic velocity from an LDV signal is described in [12]. Usually a flow propagates within the duct and the acoustic liner is flush-mounted in the lower wall. For the present experiments, the duct has been modified in such a way that the liner is placed in normal-incidence configuration and fits the whole cross-section of the duct (Figure 10).

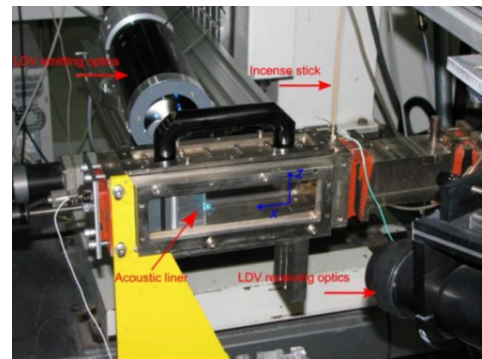


Figure 10: Experimental setup with acoustic liner. From [11]

LDV measurements have been performed at 135 dB and 3136 Hz in a plane located in the vicinity of a hole of the perforated sheet and centered on the hole axis in the transverse y direction. It is made of 15 points in each direction, and the closest line to the liner surface is located at 0.2 mm. The vortices are visualized at different time steps during a half period of signal and the flow effects observed (Figure 11).

It appears that experimental velocity fields are closely related to the ones obtained by simulations with the same scale of velocity magnitude (Figure 12). This corresponds to a weak nonlinearity. Vortices are produced at the orifice aperture but a part of the ejected mass is suctioned during flow reversal. In this case, the absorption coefficient should be slightly higher than in the linear model.

## 4 Conclusions

Applied to acoustic liners, LBM appears particularly well suited to intensive computing (eg computing with 10 to 15 million cells in a few hours). Visualization of the flow within an orifice, the development of the acoustic boundary layer and the recirculation zones appear well captured. This information is crucial to the understanding of the acoustic absorption mechanism and the implementation of suitable correction terms into the non-linear models.

Noneless, extension to configurations with grazing flow should be conducted to be representative of real application.

If successful, LBM could be used in the future to achieve the "design" of materials with a goal of linearity in a given level range.

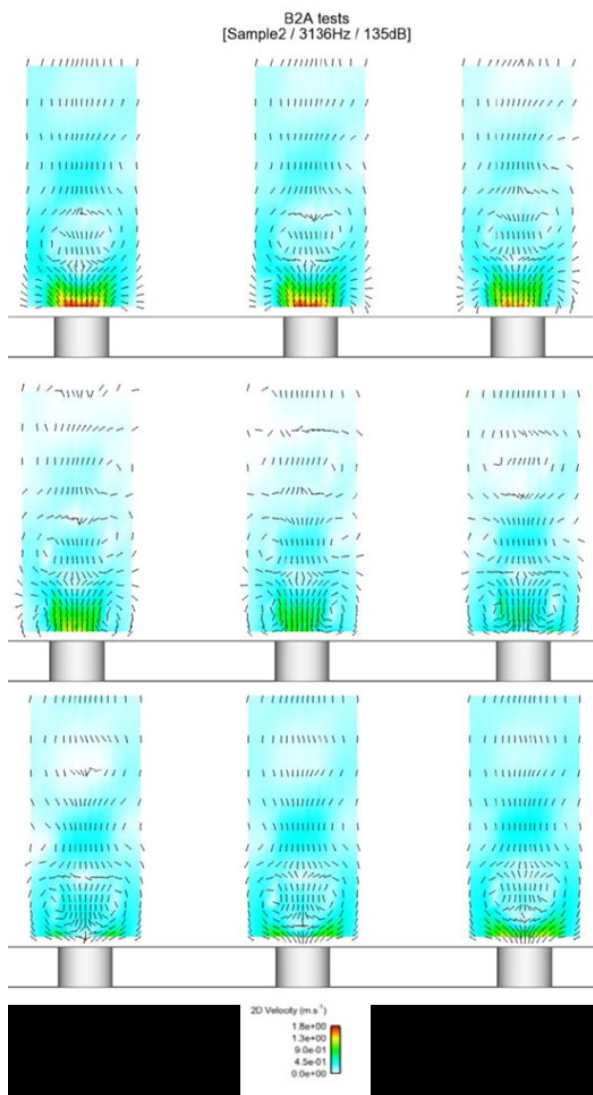


Figure 11: Measured instantaneous velocity fields obtained on Liner at 135 dB and 3136 Hz at different time steps in the half period of signal (time increasing from left to right) - From [10]

## Acknowledgments

The present work has been supported by French funded project CLIMB in the framework of the “Programme d’Investissement d’Avenir: Calcul Intensif et Simulation Numérique”.

## References

- [1] J-M. Roche, *Simulation numérique de l’absorption acoustique de matériaux résonants en présence d’écoulement*, PhD. thesis Université du Maine (2011).
- [2] Qi Zhang, D. J Bodony. Numerical investigation and modelling of acoustically excited flow through a circular orifice backed by a hexagonal cavity, *Journal of Fluid Mechanics* 693 (2012).
- [3] T. H. Melling, The acoustic impedance of perforates at medium and high sound pressure levels, *Journal of Sound and Vibration* 29.1 (1973).
- [4] M. A. Temiz et al., Non-linear acoustic transfer impedance of micro-perforated plates with circular orifices, *Journal of Sound and Vibration* 366 (2016).

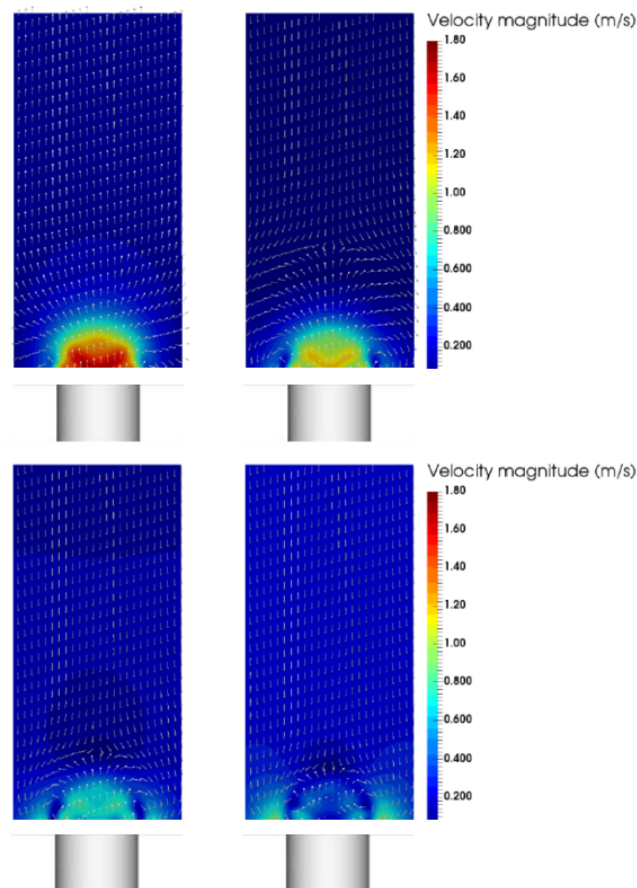


Figure 12: Simulation of instantaneous velocity fields obtained on Liner at 135 dB and 3136 Hz at different time steps in the half period of signal (time increasing from left to right).

- [5] F. Chevillotte et al., *Modeling of acoustical porous materials under flow*, SIA Automotive NVH Comfort 2016, Le Mans, 2016.
- [6] <http://www.prolb-cfd.com/>
- [7] F. Chevillotte, D. Ricot, Development and Evaluation of Non-Reflective Boundary Conditions for Lattice Boltzmann Method, 22nd AIAA/CEAS Aeroacoustics Conference, 2016.
- [8] Volunteer authors. Y plus wall distance estimation. [https://www.cfdonline.com/Wiki/Y\\_plus\\_wall\\_distance\\_estimation](https://www.cfdonline.com/Wiki/Y_plus_wall_distance_estimation).
- [9] V. Popie, *Modélisation asymptotique de la réponse acoustique de plaques perforées dans un cadre linéaire avec étude des effets visqueux*, PhD. thesis Institut Supérieur de l’Aéronautique et de l’Espace (2016).
- [10] V. Kolár, Vortex identification: New requirements and limitations, *International journal of heat and fluid flow* 28.4 (2007).
- [11] M. Lavieille, E. Piot, F. Micheli, Numerical simulations of perforate liners: Part II–Local velocity fields validation, 19th AIAA/CEAS Aeroacoustics Conference, Berlin, May 27-29 2013.
- [12] A. Minotti, F. Simon, F. Gantié, Characterization of an acoustic liner by means of Laser Doppler Velocimetry in a subsonic flow, *Aerospace Science and Technology* (2007), doi:10.1016/j.ast.2007.09.007